RSC Advances

ROYAL SOCIETY OF CHEMISTRY

www.rsc.org/advances

RSC Advances

RSCPublishing

PAPER

Surfactant-free hydrothermal fabrication of monoclinic $BiVO_4$ photocatalyst with oxygen vacancies by copper doping

Dezhi Li, Wenzhong Wang*, Dong Jiang, Yali Zheng, Xiaoman Li

Cite this: DOI: 10.1039/xoxxoooooox

Received XXXX,
Accepted XXXX

DOI: 10.1039/xoxxoooooox

www.rsc.org/

Poor electron transport leads to high recombination of photogenerated charge carriers for photocatalysts which limits the photocatalytic performance. In order to improve charge transport properties, Cu doped $BiVO_4$(Cu-$BiVO_4$) was prepared by a facile hydrothermal method. The doped material provided a maximal photocurrent 10 μA/cm^2 at +0.4 V vs SCE, which were 5 times higher than the undoped one. The result implied much improvement for separation of the carriers for Cu-$BiVO_4$, which attributed to suitable amount of oxygen vacancies as positive charge centers caused by doping. Oxygen vacancies trapped photogenerated electrons thus inhibited electrons-holes recombination. Photocatalytic degradation of rhodamine B (RhB) was used to evaluate the photoactivity of the materials. The results showed that the photocatalytic properties of the doped materials were obviously higher than undoped $BiVO_4$. The photocatalytic reaction mechanism is also discussed in this article, and the superoxide radical was confirmed to be the main active species for the photocatalytic degradation process.

1 Introduction

Because of the high rate of solar energy utilization, photocatalyst with narrow band gap (1.8-2.8 eV) is an important research region up to now. $BiVO_4$ is usually used as a pigment, but recently it has received great attention as potential candidate for highly active visible photocatalysts for the degradation of organic compounds and water oxidation.[1-3] $BiVO_4$ has three crystal phases, monoclinic $BiVO_4$ (m-$BiVO_4$) is the best one for photocatalysis with a band gap of 2.4-2.5 eV due to the transition from a valence band formed by Bi 6s or a hybrid orbital of Bi 6s and O 2p to a conduction band of V 3d. However, the poor transport rate of photogenerated electron and high recombination of photoinduced electron–hole pairs limit its application, which is attributed to the crystal structure of $BiVO_4$. The crystal structure of monoclinic $BiVO_4$ is displayed in Fig. 1, which is consists of non-interconnecting VO_4 tetrahedra. The conduction band of $BiVO_4$ mainly consists of V 3d orbitals, consequently, the photogenerated electrons have to hop between the VO_4 tetrahedrons.[4] In order to improve the charge transport properties and reduce the surface recombination of the photogenerated carriers in $BiVO_4$, great efforts have been made by doping,[5] heterojunction structure formation,[6-9] cocatalysts loading,[10-14] and nanostructures constructing.[15-17] Introduction of defects in the material by doping is a common method to change the band structure of semiconductor and bring in active sites on photocatalysts. Doping could shift semiconductor conduction band and valence energy level or form a new impurity level. This will change material surface electronic state directly, facilitate the electron-hole separation in some way,[18] and make them different in crystalline structure and morphology.[19] All of these will change their photocatalytic performance significantly. Oxygen vacancies are important active sites in catalytic reaction.[20-23] In the process of photocatalysis, trapping either electron or hole

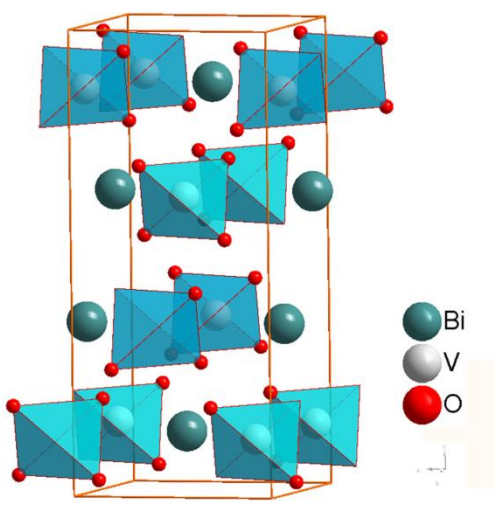

Fig. 1 The crystal structure of monoclinic $BiVO_4$.

alone is ineffective for photodegradation, because immobilized charge species recombine with mobile counterpart quickly. Trapped charges should deliver to reaction species timely. Oxygen vacancies combine the two processes very well. Their functions are mainly reflected in two aspects: they trap photogenerated electrons effectively as positive charge centers, adsorption and activation reaction species.[24]

Herein, we succeeded in introducing oxygen vacancies into $BiVO_4$ by doping Cu^{2+} (Cu-$BiVO_4$). Substitution of V^{5+} by Cu^{2+} with lower valence state could lead to extrinsic oxygen vacancies by charge compensation. It may be described by defect reactions written as:

$$2CuO \xrightarrow{V_2O_5} 2Cu_V''' + 3V_O^{\bullet\bullet} + 2O_O$$

The relationship between oxygen vacancies and photocatalytic performance of Cu-$BiVO_4$ has been investigated. Inhibition of electron-hole recombination and improvement transport rate of photogenerated charges which are expected to play a positive role in enhancing the photocatalytic activity. Photocatalytic reaction mechanism was studied, and the superoxide radical was confirmed to play a major role in photodegradation of RhB by Cu-$BiVO_4$.

2 Experimental

2.1 Preparation of Cu-$BiVO_4$ photocatalysts and their film electrodes

All reagents used in this work were analytical purity and used as received without further purification. Cu-$BiVO_4$ photocatalysts were prepared by a hydrothermal method. 2 mmol bismuth nitrate hexahydrate ($Bi(NO_3)_3 \cdot 5H_2O$) and a certain amount of $Cu(NO_3)_2 \cdot 3H_2O$, ammonium vanadate (NH_4VO_3) were dissolved in 10 mL of 2 M nitric acid, respectively. Then the above solutions were mixed together to form a stable homogeneous solution. The molar ratios of Cu to $BiVO_4$ were set as 0, 0.5%, 1.0%, 2.5%, respectively, and the corresponding products were named as Cu-0, Cu-0.5, Cu-1 and Cu-2.5. The pH values of the resulting solutions were adjusted to 8.0 with ammonia solution under constant stirring to form slurry. After being stirred for 1 h at room temperature, the slurry (about 23 mL) in the beaker was transferred to a Teflon-lined stainless steel autoclave with a capacity of 50 mL. The final capacity of slurry was adjusted to about 40 mL with deionized water and heated at 453 K for 12 h. After the autoclave was cooled to room temperature, yellow slurry was obtained. The precipitate was separated by centrifugation, washed, and dried.

Cu-$BiVO_4$ film electrodes were prepared by electrophoretic deposition on FTO substrate. The electrophoretic deposition was carried out in an acetone solution (50 mL) containing finely powder of $BiVO_4$ (40 mg) and iodine (10 mg), which was dispersed by sonication for 3 min. Two parallel FTO electrodes were immersed in the solution with a 10–12 mm distance, and a 10 V bias was applied between the two electrodes for 2 min under potentiostat (ITECHIT6834) control. The coated area was fixed at 1 cm × 1 cm. After this process, the electrode was dried and then calcined at 573 K for 1 h.

2.2. Characterization of Catalysts

The phase and composition of the as-prepared samples was examined with X-ray diffraction (XRD) recorded on a Rigaku diffraction system with Cu Kα radiation (γ = 1.5405 Å) under 40 kV and 100 mA. Survey scan was performed at a rate of 3 ° min^{-1} with 2 θ from 10° to 80°. The real Cu content in the sample was further determined by inductively coupled plasma atomic emission spectrometer (ICP-AES) analysis. The morphologies and microstructures were performed on a JEOL JEM-2100F transmission electron microscopy (TEM). UV-vis diffuse reflectance spectra (DRS) of the samples were investigated to determine their band gaps with an UV-Vis spectrophotometer (Hitachi U-3010) using $BaSO_4$ as reference. The photoluminescence spectra of the samples were recorded by a Hitachi F-4600. X-ray photoelectron spectroscopy (XPS) analysis (Thermo Scientific Escalab 250) was used to identify the elemental composition and the chemical state of Cu-$BiVO_4$.

2.3. Photocatalytic Evaluations and Photocurrent Measurements

Photodegradation of RhB in aqueous solution was carried out to

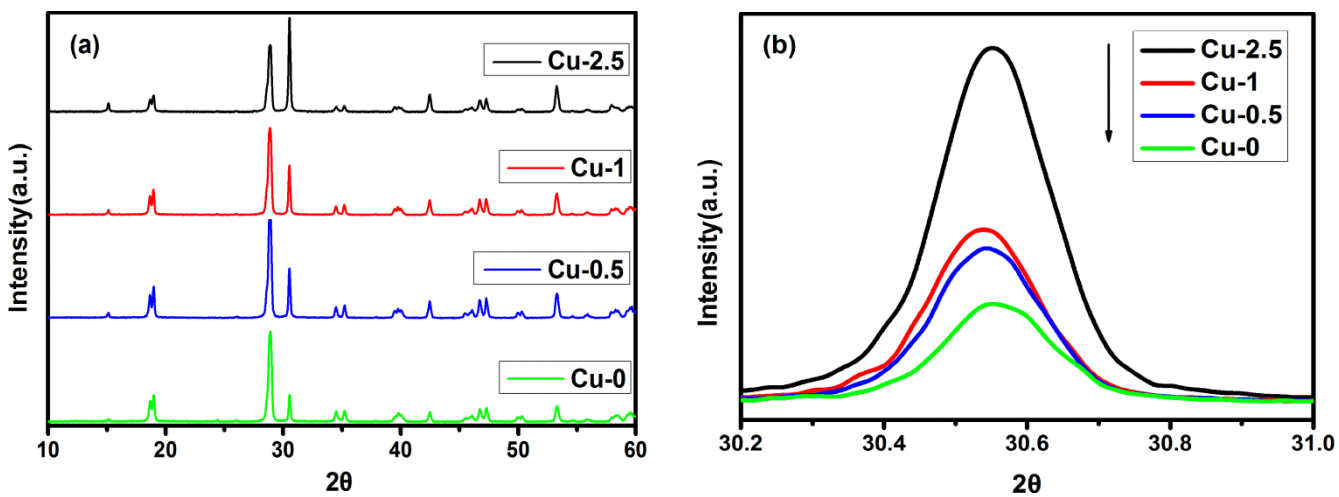

Fig. 2 (a) XRD patterns of the the as-prepared Cu-$BiVO_4$; (b) diffraction peaks of (010) facets in the range of 2θ=30.2°-31°.

evaluate photocatalytic activity of the as-prepared Cu-$BiVO_4$. Typically, 50 mg of photocatalyst was dispersed in a 100 mL solution of RhB (10^{-5} mol/L) by sonication for 1 min and magnetic stirring in the dark for 1 h to reach absorption-desorption equilibrium between RhB and the photocatalyst. After that, the solution exposed to light from a 500 W Xe lamp. At given irradiation time intervals, 2.5 mL slurry was sampled and centrifuged. The absorption spectra of the supernatant was measured by UV-Vis spectrophotometer (Hitachi U-3010) to determine the concentration change by monitoring the optical intensity of absorption spectra at 553 nm.

nitroblue tetrazolium (NBT), a probe for superoxide radical, was used to further ascertain the existence of superoxide radicals.[25] The process and conditions were similar to the former photocatalytic activity test. The NBT, exhibiting an absorption maximum at 259 nm, can be reduced by superoxide radicals. The production of superoxide radicals in the suspensions were analyzed by detecting the decrease in the concentration of NBT by UV-Vis spectrophotometer.

Photoelectrochemical performance of Cu-$BiVO_4$ electrode was measured in a three-electrode setup in a 0.1 M sodium sulphate (50 mL) by using a CHI 660 electrochemical workstation. The counter electrode was platinum electrode, and saturation mercury electrode (SCE) was used as the reference electrode. Photocurrents were measured by applying a potential to the Pt electrode using a potentiostat (EG&G). A shutter was used to record transient photocurrent decay at 20 s intervals, the photoelectric responses of the photocatalysts as light on and off were measured at +0.4 V vs SCE.

3 Results and discussion

3.1. Characterization of Cu-$BiVO_4$ photocatalyst

The compositions and crystalline phase of as-prepared material were determined by XRD test. As shown in Fig. 2, all XRD patterns of the Cu-$BiVO_4$ are assigned to monoclinic scheelite $BiVO_4$, which is in good agreement with the JCPDS standard card #14-0688. No other phase was found, which demonstrates that doping with copper does not change its phase. More (010) facet was exposed with increasing the amount of copper. The diffraction peaks for (010) facets in the range of 2θ=30.2°-31 ° are shown in Fig. 2(b), which shows that a slightly shift toward a lower anger with increasing the amount of copper. According to Bragg diffraction formula d(hkl)=λ/(2sinθ), the smaller θ is, the bigger d will be, which implies copper replaced the position of atoms with smaller ionic radius than Cu^{2+}. Correlative ionic radius, Bi^{3+} (0.108nm) > Cu^{2+} (0.72nm) > V^{5+} (0.59 nm), this determines that the shift of diffraction peak toward lower angles should cause by Cu^{2+} replaced V^{5+}.

ICP-AES, a common method for element content test, was used to further determine the real Cu content in the sample. The results were shown in table 1. The real content of copper in the two samples is about half of the usage amount in preparation. Although this values are different from the amount in preparation, but it still meets the trend what we had set. So it does not affect our judgment from the experimental results.

Table 1 The concentration of Cu in the samples before and after preparation

	usage amount in preparation	real content
Cu-1	1.0mol%	0.47mol%
Cu-2.5	2.5mol%	1.04mol%

TEM was used to investigate the surface morphology of the as-prepared Cu-$BiVO_4$ samples, and the images are displayed in Fig. 3. The as-prepared samples are mainly composed of corals-like structures. These structures were formed by assemble of nanoparticles with diameters ranging from 200 to 500 nm. Compared with undoped $BiVO_4$, no big change occurred for the particles of Cu-doped samples except smaller particle size. Smaller size for doped samples may owe to the growth of crystal was inhibited by doping of Cu in a certain extent. In the whole field of vision, any isolated CuO particles were not found.

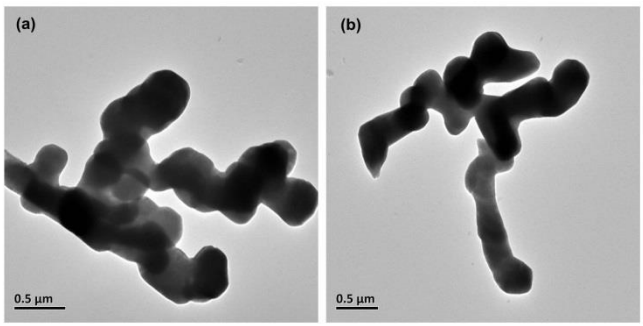

Fig. 3 TEM of the the as-prepared Cu-BiVO4, (a) Cu-0, (b) Cu-1.

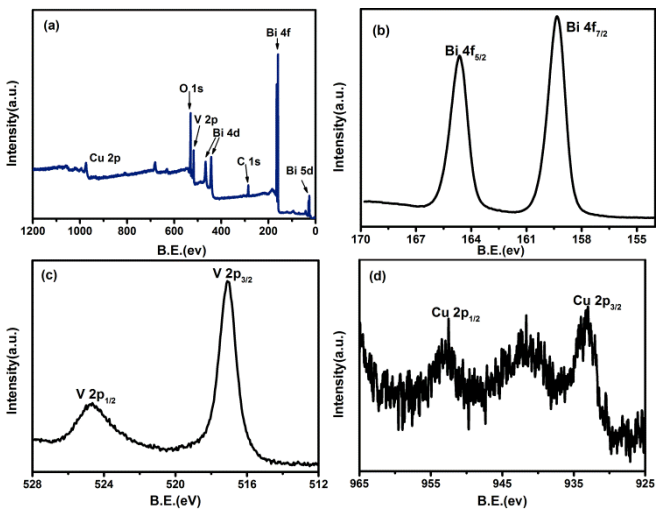

Fig. 4 XPS spectra of the the as-prepared Cu-1 (a) Overall patterns of sample ,and high-resolution XPS spectra of Cu-1 heterogeneous nanostructures: (b) Bi 4f patterns; (c) V 2p patterns and (d)Cu 2p.

X-ray photoelectron spectroscopy (XPS) was performed to understand surface components and oxidationstates of Cu-$BiVO_4$ prepared with different doping concentration. As the results shown in Fig. 4(a), all of the peaks correspond to Bi, V, O, Cu, C, respectively. C should come from the carbon tape used for XPS analysis. The high-resolution spectrum of Bi 4f

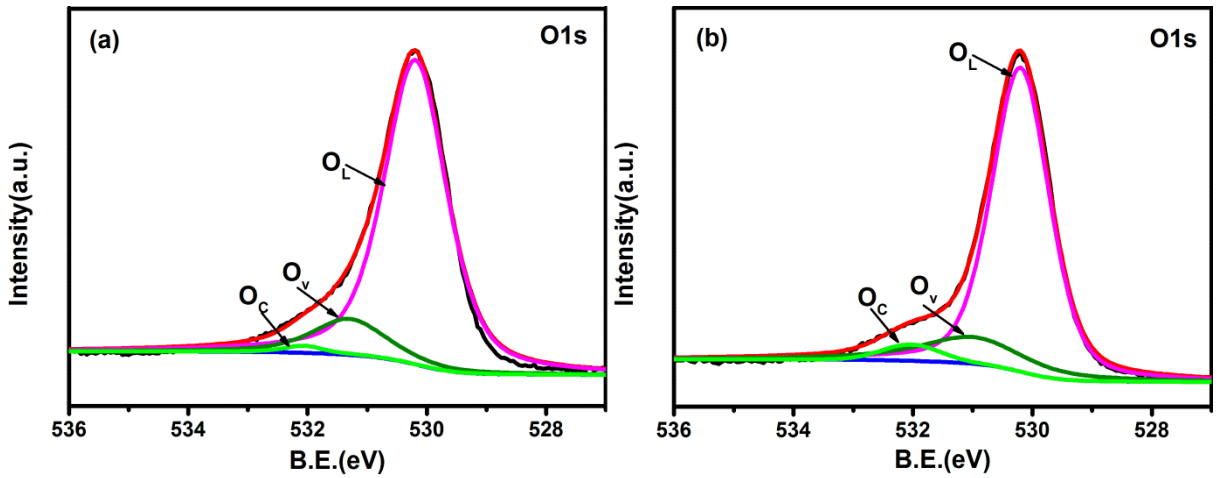

Fig. 5 Compared O 1s XPS spectra of the the as-prepared Cu-0 (a) with Cu-1 (b).

binding energy is shown in Figure 4(b), which exhibits two peaks at about 159.3 eV and 164.6 eV, correspond to the Bi 4f7/2 and Bi 4f5/2 binding energies, respectively. Fig. 4(c) shows the binding energies of the V 2p band, there are two peaks located at about 517.1 eV and 524.7 eV, which can be indexed to the V 2p3/2 and V 2p1/2 bands, respectively. Because of low concentration, two very weak peaks of Cu 2p1/2 and Cu 2p3/2 are shown in Fig. 4(d), they located at about 952.9 eV and 933.1 eV respectively, and the shake-up satellite peak at about 941.7 eV. It is evident and diagnostic of an open $3d^9$ shell of Cu^{2+}.[9]

Redox properties of photocatalyst are closely related to oxygen vacancies and chemisorbed or dissociated oxygen species on the surface of the materials. The O 1s XPS spectra of the samples are shown in Fig. 5. In general, the state of oxygen can be divided into three peaks. These peaks are associated with oxygen lattice (O_L), oxygen vacancies (O_V) and dissociated or chemisorbed oxygen species (O_C). O_C was caused by the surface chemisorbed species such as hydroxyl and H_2O.[26] Their binding energy at 530.2 eV, 531.4 eV, 532.1eV, respectively. All profiles are asymmetric and can be divided to three Gaussian features, as shown in Fig. 5. Compared with Fig. 5 (a) and Fig. 5(b), namely Cu-0 and Cu-1, the ratios of the oxygen vacancy to the total oxygen are 12.4% and 15.2%, respectively. The amount of oxygen vacancy increased a little by doping. However, the chemisorbed oxygen changed obviously. Its ratio increases from 1.4% to 3.8%, which strongly suggests the increasing of oxygen vacancies in the copper doped samples.[27]

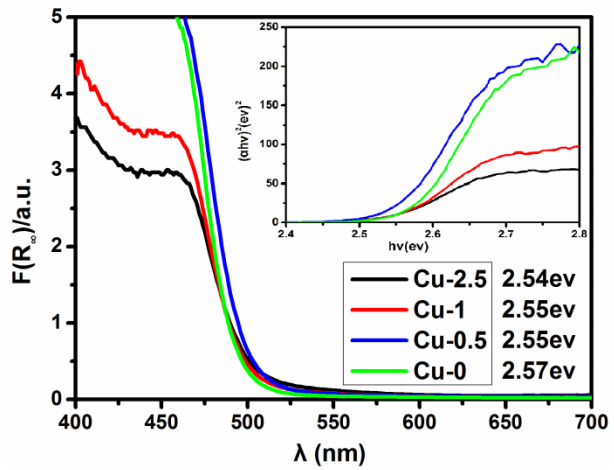

Fig. 6 UV–vis diffuse reflectance spectra (DRS) of the as-prepared samples; The insert is the plot of $(\alpha h\nu)^2$ vs. hv.

Optical absorption performance contingents on the band gap of semiconductor materials. It is considered as a key factor in determining photocatalytic performance. Fig. 6 shows the UV–Vis diffuse reflectance spectra (DRS) of Cu-$BiVO_4$ samples in comparison with pure $BiVO_4$. The as-prepared samples presented an absorption edges at about 510nm. The band gap values are shown inset of Fig. 6, the absorption edge of the samples are apparently red-shifted with increment of Cu doping concentration, so photoabsorption ability of the samples also become stronger, which may owe to oxygen vacancies were introduced by doping. Impurity bands caused by oxygen vacancies just below the bottom of conduction band, leaded to a better absorbance for photocatalyst. Cu^{2+} displaced V^{5+} with low valence state created oxygen vacancies enhanced their light absorption efficiency.

Photoluminescence (PL) analysis is regarded as a direct approach to characterize the separation efficiency of photon-generated carriers, which is closely related to photocatalytic performance. The higher PL intensity represents a higher extent of an irradiative process associated with charges recombination, and thus fewer carriers would participate in the photocatalytic reaction. Fig. 7 presents a comparison of the room temperature PL spectra of the samples Cu-0 and Cu-1 upon excitation at 340 nm.[8] Both of them exhibited a wide emission band ranges from 480 nm to 560 nm. For all the samples, three main emission peaks appeared at 519 nm, 522 nm and 529 nm. Obviously, the luminous intensity of $BiVO_4$ became weaker after doping Cu. The quenching of fluorescence shows that the recombination of photogenerated charge carriers between O 2p and V 3d were inhibited greatly

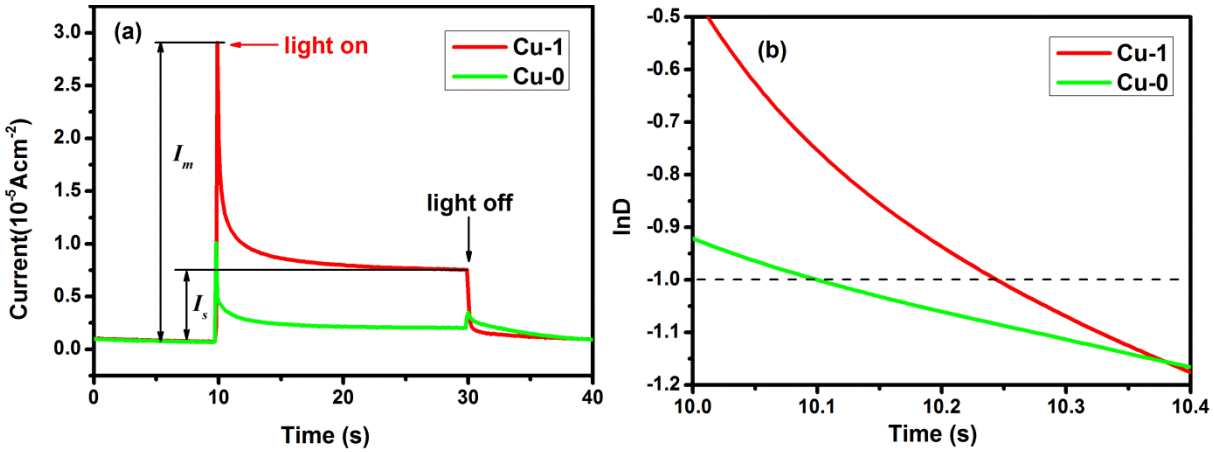

Fig. 8 (a)Transient photocurrent decay that occurs immediately upon 500W Xe lamp illumination. (b) lnD of Cu-0 and Cu-1 as functions of time.

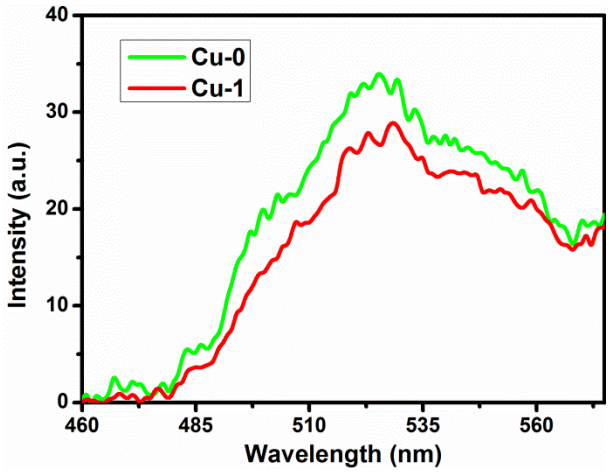

Fig. 7 Photoluminescence spectra of Cu-0 and Cu-1.

in semiconductors due to the oxygen vacancies as electron traps, which lead to a higher photon efficiency.

Bare $BiVO_4$ with poor electron transport and high bulk recombination of photogenerated charge carriers shows bad photocatalytic performance. Photocurrent measurement was used to characterize photogenerated carriers separation efficiency of photocatalysts. The photocurrent of as-prepared photocatalysts under back side illumination is shown in Fig. 8. Comparing with pure $BiVO_4$, the photocurrent of Cu-doped samples improved significantly. And Cu-1 provided a photocurrent of 10 $\mu A/cm^2$ at +0.4 V vs SCE, which are 5 times higher than bare $BiVO_4$. In general, the higher photocurrent is, the lower carrier recombination rate will be, which indicates that copper doping markedly enhanced the photogenerated carriers separation efficiency and suppressed the charge recombination. The transient photocurrent decay upon illumination was investigated. When light switched on, anodic photocurrent presented a photocurrent spike and exponential decayed rapidly to steady state. It was the result of photogenerated electron-hole quick recombination. When the light shut out, anodic photocurrent of Cu-0 produced an obvious transient overshoot and rapid attenuation, while Cu-1 appeared little overshoot. The result is shown in Fig. 8(a). The overshoot indicates the recombination was attributed to the accumulation of electrons due to the poor electron transportation in $BiVO_4$. The electronic transmission capacity of Cu-1 was improved, so obvious overshoot did not appear. The transient decay time can be calculated from a logarithmic plot of parameter D, given by the equation:

$$D = (I_t - I_s)/(I_m - I_s)$$[28]

Where I_t is the photocurrent at time t, I_m and I_s is the photocurrent spike and steady state photocurrent, respectively. lnD=-1 is defined as the transient decay time.[29] According to the previous formula, the photocurrent decay time of Cu-$BiVO_4$ and bare $BiVO_4$ can be converted to lnD as function of time, as illustrated in Fig. 8(b). The transient decay time of Cu-1 is 0.25 s, which is 2.5 times longer than Cu-0 (0.1 s), shows that Cu-1 has a slower photocurrent decay rate. Generally, the photocurrent decay rate of photocatalyst is determined by the degree of photogenerated carriers recombination. The longer transient decay time means lower rate of carriers recombination, thus more carriers can participate in photocatalytic reaction. The higher photocurrent and longer transient decay time for Cu-1 than Cu-0 may be attributed to oxygen vacancies which trap photogenerated electrons. The probability of electron-hole recombination became lower because of electrons were delivered to reaction species which were absorbed and activated by oxygen vacancies, so more carriers would migrate to the surface of photocatalyst before recombination.

3.2. Photocatalytic activity

RhB was selected as the model pollutant to study photocatalytic activity of as-prepared Cu-$BiVO_4$. Fig. 9 shows the photodegradation of RhB as a function of irradiation time in the presence of different photocatalysts. The photocatalytic performance improved obviously with Cu-doping than pure $BiVO_4$. Photocatalytic activity of the photocatalysts was strongly dependent on the copper doping concentration, and all of the doped exhibited higher efficiency. When the copper concentration increased from 0% to 1%, the photocatalytic property became higher, and Cu-1 has the best degradation performance, 95% of RhB was degraded by Cu-1 in 80 min, while pure $BiVO_4$ can only degrade 60% of RhB within the same time. When doping content was over 1%, photocatalytic activity decreased as compared with that of 1%, but still better than that of pure $BiVO_4$. This is a sign that doping with copper indeed significantly improved the photocatalytic properties of $BiVO_4$, however, it has an optimal value for doping.

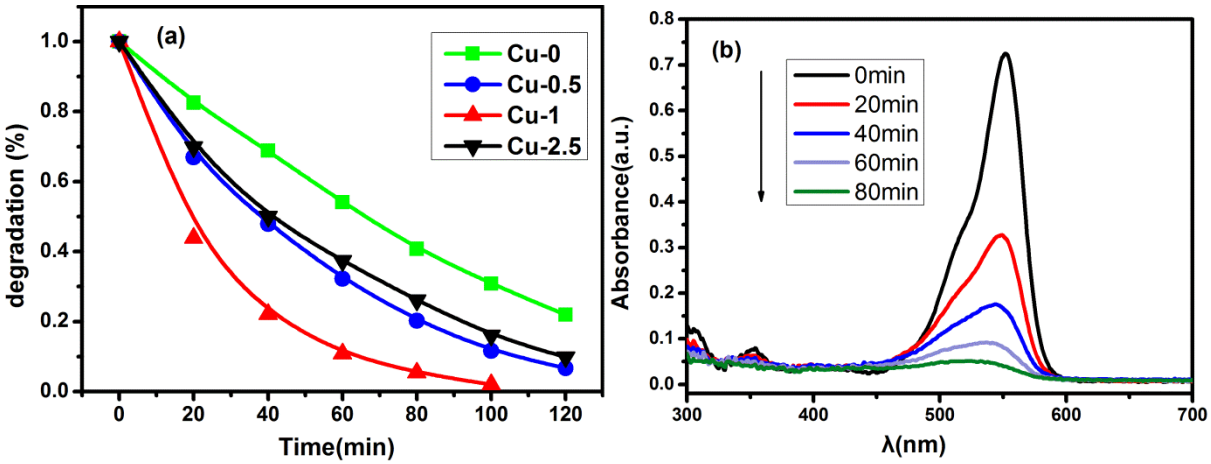

Fig. 9 (a)Photocatalytic degradation of RhB under 500W Xe lamp illumination as a function of irradiation time using the as-prepared samples. (b) The temporal evolution of the spectra during the photodegradation of RhB aqueous solution by Cu-1.

3.3. Mechanism of enhanced photocatalysis activities

$BiVO_4$ doped with copper significantly enhanced photocatalytic performance. Possible factors make these changes can be summed up in the following respects: Cu^{2+} replaced the position of V^{5+} with low valence state created oxygen vacancies. When a certain amount of copper was doped, oxygen vacancies with appropriate amount can trap the electrons, so as to limit the recombination of photogenerated carriers. The photon-generated carriers freely diffused to the active sites on photocatalyst surface where oxidation of organic species occurred. Hence, photocatalyst with appropriate content of oxygen vacancies will improve the photocatalytic performance by separating the electron–hole pairs effectively. If it exceeds the optimum value, excess oxygen vacancies will trap too many electrons. This will increase the risk of electrons contact with photon-generated holes. And this process reverse, oxygen vacancies will become recombination center. This is not conductive to the separation of electron-hole pairs. Therefore, the content of oxygen vacancies have an appropriate value, it is corresponding to an optimal value for the content of copper doping.

Photocatalytic reaction mechanism was studied in this paper. The photocatalytic reaction is a radical reaction.[9, 30, 31] Several radicals quenching agents were used to determine the mechanism of radicals. Generally, hydroxyl radicals and superoxide radicals are two major radicals involved in photocatalytic reaction. Photogenerated holes combine with water molecules generate hydroxyl radicals, and photogenerated electrons transfer to adsorbed oxygen molecules generate superoxide radicals, both of them can degrade RhB. In order to distinguish which species played a leading role in the reaction, comparative experiments for degrading RhB with Cu-1 as photocatalyst were conducted. IPA is a kind of hydroxyl radicals quenching agent.[24] IPA can remove hydroxyl radicals in the reaction system. In addition, photocatalytic degradation of RhB was carried out under N_2-saturated conditions with low concentration of superoxide radicals. The degradation of RhB experiment results are shown in Fig. 10. Degradation efficiency reduced significantly after removing two radicals. And the effect under the anoxic condition is more apparent, so it declared that the superoxide radical played a dominant role in the reaction.

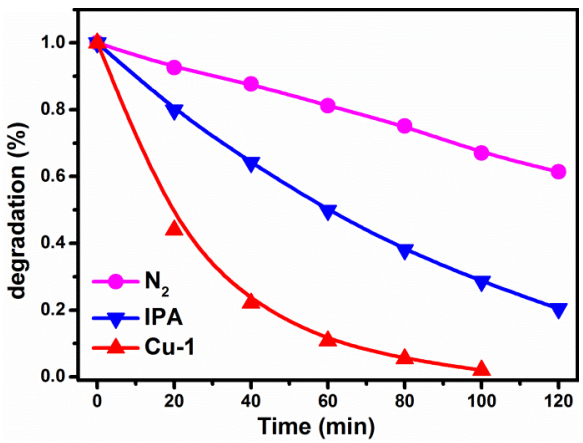

Fig. 10 Photocatalytic degradation of RhB with the addition of hydroxyl radical scavengers and in N_2-saturated solutions under Xe lamp irradiation.

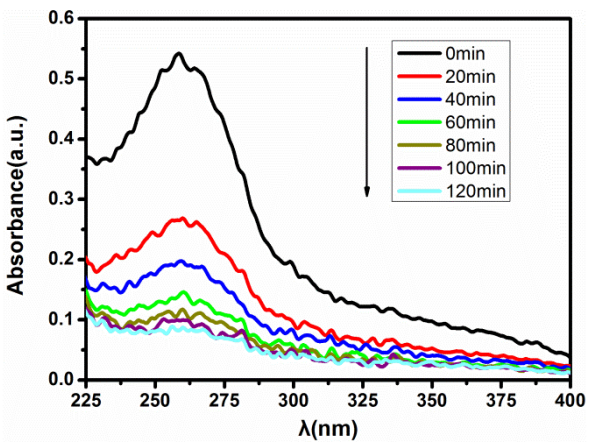

Fig. 11 UV-vis absorption spectroscopy of the solutions with NBT under Xe lamp irradiation.

Nitroblue tetrazolium (NBT), a colorless molecular probe, was chosen to further ascertain the existence of superoxide radicals. Fig. 11 shows the UV-vis absorption spectroscopy of NBT after different irradiation time in the photocatalytic reaction by Cu-1. The decrease of NBT concentration indicates the

production of superoxide radicals in degradation process. The path of the degradation reaction can be described as follows: oxygen vacancies on the surface of photocatalyst particularly exposed to the air and adsorbed oxygen molecules; photocatalyst was irradiated by incident light then released electrons and holes; the positively charged oxygen vacancies drawn the photoproduction electrons, they worked as electron acceptors by electrostatic force, the electrons were transferred to oxygen molecules which were absorbed on oxygen vacancies and generated superoxide radicals; then superoxide radicals reacted with RhB, and the products were water and carbon dioxide.

4 Conclusions

Cu doped $BiVO_4$ was prepared by a facile templates-free hydrothermal reaction without any additional surfactants. Successful introduction of oxygen vacancies in the material significantly improved the performance of the photocatalytic degradation of RhB. And the effect of oxygen vacancies in the process of photocatalytic reaction was verified. This article provides a strategy for the development of efficient photocatalysts.

Acknowledgements

We acknowledge the financial support from the National Basic Research Program of China (2013CB933203) and the National Natural Science Foundation of China (51272269, 51272303, and 51102262).

Notes and references

State Key Laboratory of High Performance Ceramics and Superfine Microstructures, Shanghai Institute of Ceramics, Chinese Academy of Sciences, 1295 Dingxi Road, Shanghai 200050, P. R. China
E-mail: wzwang@mail.sic.ac.cn

1. X. Lang, W. Ma, C. Chen, H. Ji and J. Zhao, *Acc. Chem. Res.*, 2013, 47, 355-363.
2. X. Lang, X. Chen and J. Zhao, *Chem. Soc. Rev.*, 2014, 43, 473-486.
3. A. Kudo and Y. Miseki, *Chem. Soc. Rev.*, 2009, 38, 253-278.
4. Y. Park, K. J. McDonald and K. S. Choi, *Chem. Soc. Rev.*, 2013, 42, 2321-2337.
5. B. Zhou, X. Zhao, H. Liu, J. Qu and C. P. Huang, *Appl. Catal. B.*, 2010, 99, 214-221.
6. N. Wetchakun, S. Chaiwichain, B. Inceesungvorn, K. Pingmuang, S. Phanichphant, A. I. Minett and J. Chen, *ACS Appl. Mater. Interfaces*, 2012, 4, 3718-3723.
7. Z. He, Y. Shi, C. Gao, L. Wen, J. Chen and S. Song, *J. Phys. Chem. C*, 2014, 118, 389-398.
8. C. Yu, K. Yang, J. C. Yu, F. Cao, X. Li and X. Zhou, *J. Alloys Compd.*, 2011, 509, 4547-4552.
9. W. Wang, J. Wang, Z. Wang, X. Wei, L. Liu, Q. Ren, W. Gao, Y. Liang and H. Shi, *Dalton Trans.*, 2014, 43, 6735-6743.
10. R. Li, H. Han, F. Zhang, D. Wang and C. Li, *Energ. Environ. Sci.*, 2014, 7, 1369-1376.
11. S. Ho-Kimura, S. J. A. Moniz, A. D. Handoko and J. Tang, *J. Mater. Chem. A*, 2014, 2, 3948-3953.
12. D. Wang, R. Li, J. Zhu, J. Shi, J. Han, X. Zong and C. Li, *J. Phys. Chem. C*, 2012, 116, 5082-5089.
13. G. K. Fu, G. N. Xu, S. P. Chen, L. Lei and M. L. Zhang, *Catal. Commun.*, 2013, 40, 120-124.
14. R. Li, F. Zhang, D. Wang, J. Yang, M. Li, J. Zhu, X. Zhou, H. Han and C. Li, *Nat. Commun.*, 2013, 4, 1432.
15. G. Xi and J. Ye, *Chem. Commun.*, 2010, 46, 1893-1895.
16. S. Obregon and G. Colon, *J. Mol. Catal. A-Chem.*, 2013, 376, 40-47.
17. G. Q. Tan, L. L. Zhang, H. J. Ren, S. S. Wei, J. Huang and A. Xia, *ACS Appl. Mater. Interfaces*, 2013, 5, 5186-5193.
18. K. P. S. Parmar, H. J. Kang, A. Bist, P. Dua, J. S. Jang and J. S. Lee, *ChemSusChem*, 2012, 5, 1926-1934.
19. S. Usai, S. Obregón, A. I. Becerro and G. Colón, *J. Phys. Chem. C*, 2013, 117, 24479-24484.
20. R. Schaub, P. Thostrup, N. Lopez, E. Laegsgaard, I. Stensgaard, J. K. Norskov and F. Besenbacher, *Phys. Rev. Lett.*, 2001, 87, 266104.
21. J. Gan, X. Lu, J. Wu, S. Xie, T. Zhai, M. Yu, Z. Zhang, Y. Mao, S. C. Wang, Y. Shen and Y. Tong, *Sci. Rep.*, 2013, 3, 1021.
22. M. Xing, W. Fang, M. Nasir, Y. Ma, J. Zhang and M. Anpo, *J. Catal.*, 2013, 297, 236-243.
23. F. Zuo, L. Wang, T. Wu, Z. Y. Zhang, D. Borchardt and P. Y. Feng, *J. Am. Chem. Soc.*, 2010, 132, 11856-11857.
24. Z. J. Zhang, W. Z. Wang, E. P. Gao, M. Shang and J. H. Xu, *J. Hazard. Mater.*, 2011, 196, 255-262.
25. A. Y. Booshehri, S. C.-K. Goh, J. Hong, R. Jiang and R. Xu, *J Mater. Chem. A*, 2014, 2, 6209-6217.
26. X. Zhang, J. Qin, Y. Xue, P. Yu, B. Zhang, L. Wang and R. Liu, *Sci. Rep.*, 2014, 4, 04596.
27. H. Jiang, H. Dai, X. Meng, K. Ji, L. Zhang and J. Deng, *Appl. Catal. B.*, 2011, 105, 326-334.
28. Y. Wang, C. Feng, M. Zhang, J. Yang and Z. Zhang, *Appl. Catal. B.*, 2010, 100, 84-90.
29. L. Zhang, E. Reisner and J. J. Baumberg, *Energ. Environ. Sci.*, 2014, 7, 1402-1408.
30. N. J. Bell, Y. H. Ng, A. Du, H. Coster, S. C. Smith and R. Amal, *J. Phys. Chem. C*, 2011, 115, 6004-6009.
31. Y. Zhao, W. Ma, Y. Li, H. Ji, C. Chen, H. Zhu and J. Zhao, *Angew. Chem. Int. Ed.*, 2012, 51, 3188-3192.
32. J. Xu, W. Z. Wang, M. Shang, E. P. Gao, Z. J. Zhang and J. Ren, *J. Hazard. Mater.*, 2011, 196, 426-430.